Reviews of Electromagnetics, Vol. IV, 2025
EuCAP 2025 Special Issue
DOI: 10.53792/RoE/2025/25004

Reviews of Electromagnetics
EuCAP 2025 Special Issue

A Comparative Analysis of 3D Printed Substrate and Laminate-Based Rectangular Patch Antennas at C-Band

Saúl S. Carvalho[1,2], João R. Reis[2,1] and Rafael F. S. Caldeirinha[1,2*]

Abstract
This paper presents a comparative study between 3D printed and laminate-based rectangular patch antennas, specifically designed to operate at 4.7 GHz. A total of five patch antennas, fabricated using additive manufacturing (AM) techniques and several materials as substrates (Nanoe Zetamix Epsilon filaments, PETG and PLA), are compared against four antenna prototypes made in well known laminate substrates (FR4, Rogers RT/duroid 5880, RO4350B, and RT/duroid 6010LM). For the 3D printed antenna prototypes, different metallisation techniques, including copper foil, silver spray, and silver cloth tape, were employed to enhance the electrical performance of the antennas. The results show that the 3D printed antennas performed reasonably well compared to their laminate counterparts, although several challenges were encountered, particularly related to manufacturing inconsistencies and the brittleness of the Zetamix filaments.

Key terms
3D printing; 3D printed, antenna, Additive manufacturing.

[1] *Polytechnic of Leiria, Leiria, Portugal*
[2] *Instituto de Telecomunicações, Leiria, Portugal*
*__Corresponding author__: rafael.caldeirinha@ipleiria.pt

Received: 19/05/2025, Accepted: 04/12/2025, Published: 08/12/2025

1. Introduction

Additive manufacturing (AM) techniques, complemented by methods such as metallisation, allow for the design of various antenna types applicable across multiple industries. Three-dimensional (3D) printing offers a rapid development process, enabling the construction of complex antenna components and configurations while providing better cost control compared to traditional manufacturing techniques. This cost-effectiveness also makes AM a valuable approach for developing low-budget antennas, ideal for hands-on teaching applications and for deployment in resource-limited regions or developing countries.

Several examples of 3D printed antennas are presented in studies [1–10], showcasing a wide variety of applications and fabrication methods. For example, in [1], *Pizarro et al.* explored the influence of various additive manufacturing parameters using conductive filaments for microwave devices, emphasizing the importance of print quality and filament selection in achieving functional electromagnetic performance. In [2], it is demonstrated the design of ultra-wideband flat metamaterial gradient-index (GRIN) lenses enabled by additive manufacturing, which significantly improved focusing capability and beam shaping in antenna systems. Furthermore, the work in [3] presents a 3D-printed gradient-index Luneburg lens that converts linear polarization into dual-circular polarization for multi-beam applications. The proposed lens operates from 12.6–17.1 GHz and achieves beam scanning up to $\pm 60^{\circ}$ using five feeds. Measurements show a 30% bandwidth with $S_{1,1}$ below –10 dB and axial ratios under 3 dB. The gradient-index material lens typically involves exploring the infill type of the 3D-printed material to achieve specific effective dielectric properties, which are useful in producing such designs, as reported in [11]. Using a different approach, the work [4] introduced a compact monoblock parabolic reflector antenna aimed at K-band radar applications, highlighting the advantages of 3D printing in producing low-cost and high-performance reflectors. The antenna consisted of a traditional parabolic antenna assembly, in which the reflector was 3D printed in dielectric material and metallised with aluminium foil. The authors achieved 18 dBi of gain at 24.125 GHz for an antenna with overall dimensions of $60 \times 60 \times 21$

mm^3. Alternatively in [5], it is presented a sub-terahertz *Luneburg* lens antenna using metallic surface-wave structures, pushing the boundaries of 3D printing into higher frequencies with multilayer designs. *Stoumpos et al.* [6] developed a conformal slotted waveguide array through additive manufacturing, enabling lightweight, compact, and conformal solutions for aerospace and vehicular platforms. The study in [7] focused on evolutionary-optimized Wi-Fi antennas produced through laser powder bed fusion, illustrating the synergy between advanced optimization algorithms and high-resolution metal 3D printing. Finally, [8] proposed a wideband Cassegrain antenna featuring a concave subreflector for 5G millimeter-wave multibeam applications, demonstrating the feasibility of printing intricate reflector profiles for modern communication systems. Several other examples of 3D printed antennas and techniques can be found in our literature review publication [12].

While these studies highlight the versatility and increasing maturity of 3D printing in enabling a wide range of high-performance, application-specific antenna designs, the potential of AM is further expanded by the emergence of four-dimensional (4D) printing. This innovative approach incorporates smart materials that allow antennas to adapt their physical structure or electromagnetic performance in response to external stimuli such as temperature, light, or humidity. As reported in [13], such adaptive 4D printed antennas can dynamically modify their characteristics, paving the way for reconfigurable and environmentally responsive antenna systems.

This article investigates Fused Deposition Modelling (FDM) 3D-printed and laminate-based rectangular patch antennas, specifically targeting a central frequency of 4.7 GHz. Such antennas can be employed in a wide range of applications, including the 5G New Radio (NR) n79 band. This frequency was selected as it lies at the upper end of the 5G NR Frequency Range 1 (FR1), offering wider bandwidths compared to the lower FR1 bands and therefore presenting a worst-case scenario for assessing antenna performance within the specified range. Additionally, this choice aligns with the available equipment for extracting the complex relative permittivity (ε_r) of dielectric materials in the 4–6 GHz range.

A key motivation of this work is to explore the feasibility of fabricating antennas using alternative methods for both the substrate and the metallisation of the radiating elements. Specifically, it aims to compare traditional patch antennas, commonly manufactured using printed circuit board (PCB) techniques and commercial laminates such as FR4, Rogers RT/duroid 5880, RO4350B, and RT/duroid 6010LM, with antennas produced through 3D printing in several dielectric filaments and various metallisation strategies. Demonstrating that these alternative methods can yield viable antennas would not only provide a cost-effective fabrication approach but also position additive manufacturing as a compelling solution for developing low-budget antennas.

This paper is organised as follows: Section 2 presents the antennas design and modelling considerations; Section 3 details fabrication of the antennas; Section 4 presents a comparative analysis between the electromagnetic simulations and measurements obtained for every antenna model. Finally, in section 6, the main conclusions are drawn.

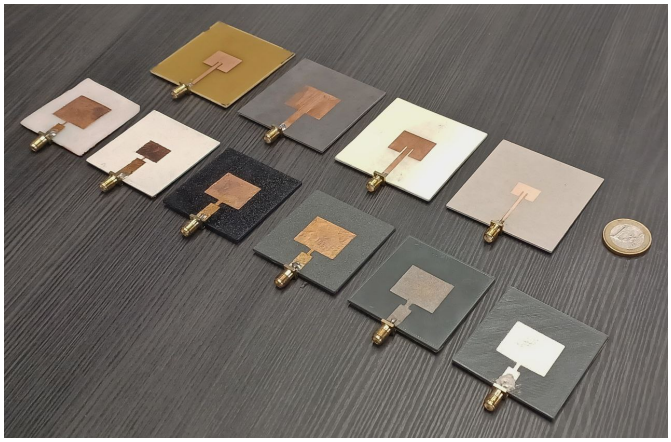

Figure 1: The ten fabricated patch antennas, with the four laminate patch antennas line on the top and six metallised 3D printed antennas lined on the bottom.

2. Antenna Design and Modelling Considerations

For this comparative study, a total of 10 patch antennas were simulated in CST MWS and further fabricated for electromagnetic (EM) characterisation. The antennas were designed following traditional rules for microstrip patches [14]. The fabricated prototypes are depicted in Fig. 1 and further detailed in Fig. 2 and Fig. 5, for laminate base and 3D printed substrate base, respectively.

The laminate based antennas, named A1 to A4 and represented in Fig. 2 (a) to (d), were fabricated by standard etching techniques, using 4 different substrates: Bungard FR4, and Rogers RT/duroid 5880, RO4350B, and Rogers RT/duroid 6010LM, respectively. On the other hand, the 3D printed antennas depicted in Fig. 5 (a) to (f), named A5 to A10, were based on substrates fabricated using 3D printing of several filament types, which were further metallised manually using different methods including: stamped copper foil, silver spray coating, and glued silver fabric tape. Although certain filaments such as ABS, ASA, or Nylon exhibit dielectric properties more comparable to high-permittivity laminates (e.g., RO4350B or RO6010LM), they were not considered in this study due to their demanding printing requirements, including the need for enclosed heated chambers and direct-drive extrusion systems. Instead, commonly available and easier-to-print filaments such as PLA and PETG were selected to ensure reproducibility and to reflect the practical capabilities of standard FDM 3D printers.

Table 1, summarises the combinations of methods and materials utilised for both the laminate and the 3D printed antennas, including the dielectric properties of the substrates and the conductivity values of the considered metallic materials. The dielectric properties of the substrates for all the antennas were obtained from the supplier's datasheets, when available. For the non-characterised 3D printed materials, the ε_r was obtained by measurements carried out in material samples using two-port waveguide permittivity extraction between 4-6 GHz using WR187 standards [15, 16].

As already mentioned, several materials have been consid-

Table 1: Substrate and metallisation combinations for the laminated and 3D printed antennas.

Reference	Denomination	Cladding Material	Substrate Material	Cladding Parameters	Substrate Parameters	
				σ (S/m)	ε_r'	$tan\delta$
A1	Bungard FR4	Copper	FR4	58.0×10^6	4.50 *	0.0150 *
A2	Rogers 5880	Copper	Rogers	58.0×10^6	2.20 ‡	0.0009 ‡
A3	Rogers 4350B	Copper	Rogers	58.0×10^6	3.48 ‡	0.0037 ‡
A4	Rogers 6010LM	Copper	Rogers	58.0×10^6	10.2 ‡	0.0023 ‡
A5	PETG + Copper Foil	Copper Foil	PETG	58.0×10^6	2.60 $^△$	0.01 $^△$
A6	PLA + Copper Foil	Copper Foil	PLA	58.0×10^6	2.65 $^△$	0.01 $^△$
A7	PLA + Silver Fabric	Silver Fabric	PLA	0.20×10^6	2.65 $^△$	0.01 $^△$
A8	PLA + Silver Coating	Silver Coating	PLA	0.45×10^6	2.65 $^△$	0.01 $^△$
A9	Zetamix ε = 2.2 + Copper Foil	Copper Foil	Zetamix ε = 2.2	58.0×10^6	2.20 †	0.0011 †
A10	Zetamix ε = 7.5 + Copper Foil	Copper Foil	Zetamix ε = 7.5	58.0×10^6	7.50 †	0.0011 †

$\triangle$ - adapted from ε_r extraction measurements and literature for similar materials;
Datasheet measurements at: 1 GHz ($*$), 9.4 GHz (†) and 10 GHz (‡).

ered for the metallic parts of the 3D printed patch antennas (Table 1), which include the ground plane, the feeding and radiating elements. When copper foil is employed, an electrical conductivity (σ) of 58.0×10^6 S/m is considered. This corresponds to the conductivity value set as default settings in CST MWS. The copper foil was measured with a thickness of 50 μm using a micrometer. The skin depth (δ) was calculated to be 0.95 μm at 4.7 GHz, for a relative permeability (μ_r) of 0.999991 [17]. The yielded δ value confirms that the conductor thickness is more than sufficient for optimal electrical conductivity at 4.7 GHz. On the other hand, silver coating spray (MG Chemicals 843AR - $\sigma = 0.455\times10^6$ S/m [18]) was also employed to metallise the patch antennas. Two coats of 843AR spray were applied, resulting in an expected thickness of 101.6 µm, according to [18]. This silver spray has an electrical resistivity (ρ) of 2.198×10^{-6} Ω·m [18], translating to a $\delta = 10.88$ μm at 4.7 GHz, based on silver's permeability of 0.99998 [17]. Silver cloth tape was also utilised for antenna metallisation, typically exhibiting a resistance of approximately 0.05 Ω [19, 20]. The 50 mm silver cloth tape used for antenna fabrication was measured at a thickness of 100 μm, resulting in $\rho = 5\times10^{-6}$ Ω·m and $\sigma = 0.200\times10^6$ S/m. Based on silver's permeability [17], the silver cloth tape has a δ of 16.42 μm at 4.7 GHz, confirming that its thickness is also sufficient for the antenna fabrication.

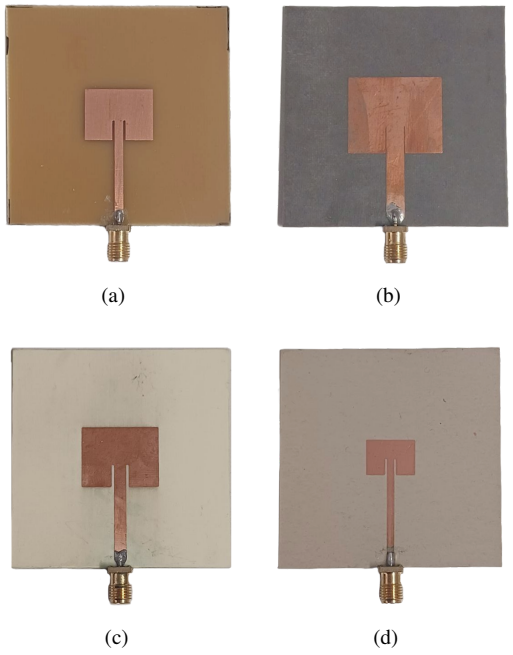

Figure 2: Fabricated laminate patch antennas: Bungard FR4 - A1 (a), Rogers RT/duroid 5880 - A2 (b), Rogers RO4350B - A3 (c), and Rogers RT/duroid 6010LM - A4 (d).

3. Antenna Design and Fabrication

After researching on different materials and fabrication processes, the patch antennas were then designed and optimised using CST Microwave Studio before being sent for production. This section describes the antenna layouts and the fabrication process for each model of antenna.

3.1. Laminate Patch Antennas

The laminate patch antennas, A1 to A4 (Fig. 2), were designed according to width (W), length (L) and height (h) dimensions for the different elements (Fig. 3) where W_g and L_g refer to the ground plane, W_p and L_p refer to the patch element, W_c and L_c refer to the patch inset feed cuts, W_f and L_f refer to the transmission line, W_{pin} and L_{pin} refer to the SMA connector pin, h_{sub} to the substrate's height and h_{clad} to the cladding's height. The radius of the SMA pin is 0.45 mm thus the W_{pin} (diameter of the pin) being 0.9 mm while L_{pin} has a length of 4mm. A summary of the dimensions of each laminate patch antenna can be found in Table 2.

The fabrication process for A1, shown in Figure 2 (a) began by cutting the board and cleaning the copper cladding with steel wool. Acetate sheets with printed designs were aligned on both sides, followed by one minute of UV exposure, which protected the pre-sensitised copper. The board was then developed in sodium hydroxide to remove photoresist from the exposed areas, etched with iron perchlorate to remove the exposed copper, cleaned, and finally coated with silicone isolation spray.

For the Rogers antennas, A2 (b) to A4 (d), whose boards were not pre-sensitised, the process involved similar initial steps: cutting and cleaning. Photosensitive dry film was applied to both sides, with proper adhesion ensured using a laminator. A negative acetate mask was aligned, and UV exposure protected the copper beneath the exposed areas of the film, as shown after exposure in Fig. 4. After removing the second layer of dry film, the boards underwent the same etching, cleaning, and

Table 2: Summary of dimensions for each laminate patch antenna in millimetres.

Antenna Reference	W_g	L_g	W_p	L_p	W_f	L_f	W_c	L_c	h_{sub}	h_{clad}
A1	60.00	60.00	18.96	14.34	2.48	22.83	0.51	5.51	1.520	0.0350
A2	60.00	60.00	25.10	20.51	4.55	19.75	0.15	7.49	1.575	0.0175
A3	60.00	60.00	20.98	16.26	3.08	21.87	0.12	6.10	1.520	0.0350
A4	60.00	60.00	13.02	9.37	1.76	25.32	0.07	3.90	1.270	0.0175

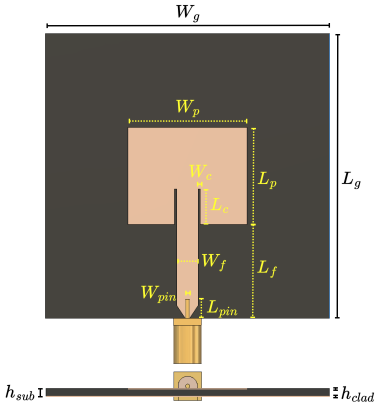

Figure 3: Rectangular patch antenna model using the inset feed impedance matching technique.

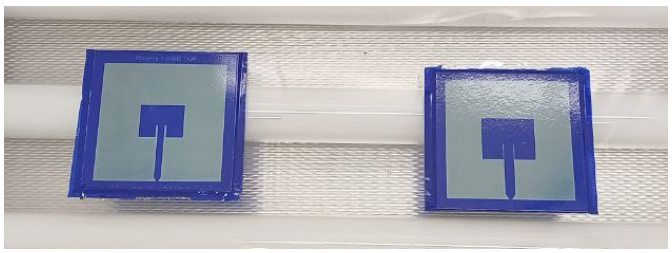

Figure 4: Two of the Rogers patch antennas after UV exposure.

protection steps as the FR4 board. This ensured both types of boards achieved the precise patterns needed for optimal antenna performance.

3.2. 3D Printed Patch Antennas

As referenced in [14], microstrip patch antennas can employ various impedance matching techniques. Initially, all patch antennas were intended to be designed using the inset feed method, as was done for the laminate-based models. However, it quickly became apparent that accurately replicating this technique manually for the 3D-printed antennas was unfeasible, due to the difficulty in precisely cutting the inset feed gaps. Consequently, a $\lambda/4$ transformer was employed for the 3D-printed patch antennas. The 3D-printed antennas, labelled A5 to A10 (Fig.5), were therefore designed using the same parameters as those shown in Fig.3, except for the change in matching technique. The dimensions W_t and L_t refer to the width and length of the $\lambda/4$ transformer, respectively, as illustrated in Fig. 6. A summary of the optimised dimensions for each 3D-printed patch antenna is provided in Table 3.

To fabricate the antennas, the substrates were printed using various filament materials, including standard Polyethylene Terephthalate Glycol (PETG) and Polylactic Acid (PLA), and an electromagnetically characterised Zetamix filament. Printing was performed on a Bambu Lab X1C printer, with a layer resolution of 0.2 mm and 100 % of material infill.

To metallise the radiating elements and ground planes, antennas A5, A6, A9, and A10, shown in Figures 5 (a), (b), (e), and (f), respectively, were fabricated by applying copper foil tape to both sides of the printed substrates. A 3D-printed mould of the radiating patch, including the $\lambda/4$ transformer, was used to accurately cut the required shape, as shown in Fig. 7.

Antenna A7 (Fig.5 (c)) followed a similar cutting process but used silver fabric cloth tape, which was then adhered to the substrate. In contrast, antenna A8 (Fig.5 (d)) was fabricated using a "negative mould" to apply silver spray onto the ground plane, patch, and transmission line.

For all the antennas metallised with copper tape, the SMA connector was carefully solder using solder wire and a solder iron, to avoid melting the 3D printed substrate. For antennas A7 (silver fabric) and A8 (silver-coated), silver conductive glue, commonly used in PCB repair, was employed to attach the SMA connectors, as soldering was not feasible for these materials.

However, for the silver-coated antenna (A8), poor radiation performance was quickly observed, likely due to insufficient coating thickness, presumably caused by uneven spray application, which was not enough to ensure adequate skin depth.

Table 3: Summary of dimensions for each 3D printed patch antenna in millimetres.

Antenna Reference	W_g	L_g	W_p	L_p	W_f	L_f	W_t	L_t	h_{sub}	h_{clad}
A5	50.00	50.00	23.96	19.14	6.5	15.43	1.5	4.00	1.63	0.05
A6	50.00	50.00	23.79	18.96	6.5	15.52	1.5	4.00	1.63	0.05
A7	50.00	50.00	23.96	19.14	6.5	15.43	2.0	4.00	1.63	0.10
A8	50.00	50.00	23.90	19.09	6.0	15.45	1.5	4.00	1.63	0.06
A9	50.00	50.00	25.44	20.76	6.0	14.61	1.0	3.92	1.60	0.05
A10	50.00	50.00	18.57	13.99	6.0	18.01	1.0	5.48	1.60	0.05
A11	50.00	50.00	15.90	11.55	7.0	19.22	1.0	2.65	1.60	0.05

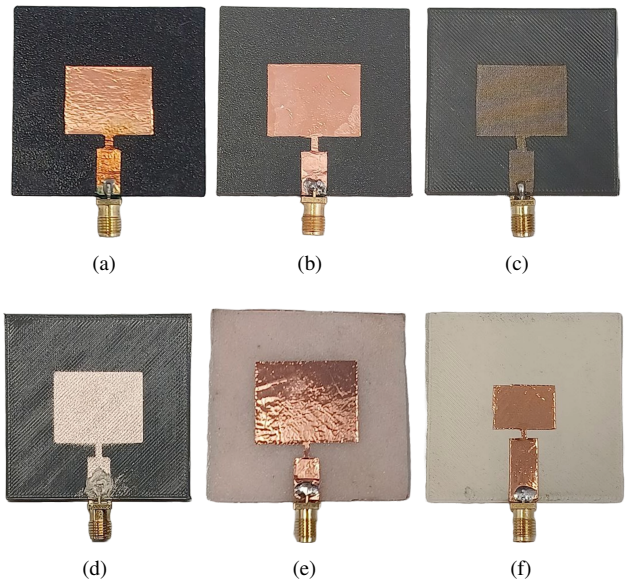

Figure 5: Fabricated 3D printed patch antennas: black PETG and copper foil - A5 (a), gray PLA and copper foil - A6 (b), gray PLA and silver fabric tape - A7 (c), gray PLA and silver coating spray - A8 (d), Zetamix $\varepsilon = 2.2$ and copper foil - A9 (e), and Zetamix $\varepsilon = 7.5$ and copper foil - A10 (f).

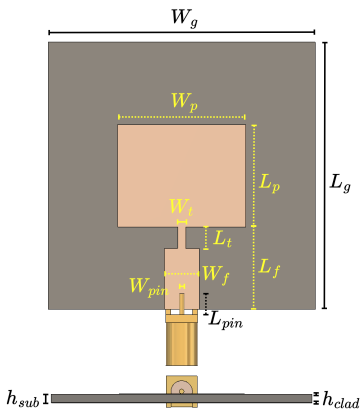

Figure 6: Patch antenna model using the $\lambda/4$ transformer impedance matching technique.

To address this issue, silver cloth tape was added to the ground plane for extra metallisation. While the coating caused an upward resonance shift, the silver tape brought the resonance frequency closer to the target 4.7 GHz, though impedance matching remained poor.

4. Electromagnetic Simulations and Measurements

For the electromagnetic simulations, all the antenna models were designed in CST MWS. Each model incorporated an SMA connector at the input, excited via a waveguide port. Open boundary conditions were applied. For each model, the impedance matching (S_{11}), bandwidth (based on the -10dB threshold) and realised gain were analysed over the 4–6 GHz frequency range. Total efficiency was evaluated at 4.7 GHz.

It should be noted that, in the electromagnetic simulations, all layers were modelled as perfectly smooth and uniform sheets.

Figure 7: Example of one of the 3D printed patch antennas mould and cutting process.

Figure 8: Depiction of the measurement setup inside the anechoic chamber.

Surface roughness either arising from the manual metallisation processes (e.g., stamped or glued conductive foils) or due to layering of 3D printing were not considered. This simplification may contribute to some of the discrepancies observed between simulated and measured results.

Subsequent optimisations within CST Studio focused on enhancing impedance matching between the transmission line and the patch. Additional adjustments were made to shift the resonance frequency precisely to 4.7 GHz, ensuring optimal performance for the intended application, resulting in the dimensions already presented in Tables 3 and 2, for laminate-base and 3D-printed base antennas, respectively.

After prototyping, the measurements were conducted in an anechoic chamber using a Vector Network Analyser (VNA) and a custom setup featuring a collaborative robot. A tailored patch antenna support was designed to securely hold each of the fabricated patches during testing. The setup enabled azimuth and elevation radiation pattern cross-section measurements, ranging from -180 to 180°, and -15 to 15°, respectively. The measurement setup can be seen in Fig. 8. The EM absorbers were temporarily removed from the robotic gripper for photographic purposes.

4.1. Laminate Patch Antennas

Among the fabricated prototypes, the laminate patch antennas exhibit the closest agreement with simulation results when compared to their 3D printed counterparts, as further discussed in the following subsection. The measured S_{11} responses exhibit relatively good impedance matching across all measured antennas. However, slight shifts in the resonance frequency are observed for the Rogers RO4350B and Rogers 6010LM designs, likely due to minor over-etching during fabrication, particularly around the corners of the patches. The simulated and measured S_{11} parameters, along with the realised gain for the laminate patch antennas, are presented in Fig. 9.

Using the S_{11}, realised gain, directivity, and effective area, the reflection and radiation efficiencies of the laminate patch antennas were calculated, as depicted in Fig. 10. The total efficiency of the laminate patch antennas was obtained by processing the reflection and radiation efficiencies further. The measured values align closely with the simulated results, exhibiting only minor deviations when accounting for the previously discussed factors.

The azimuth and elevation cross-section radiation pattern

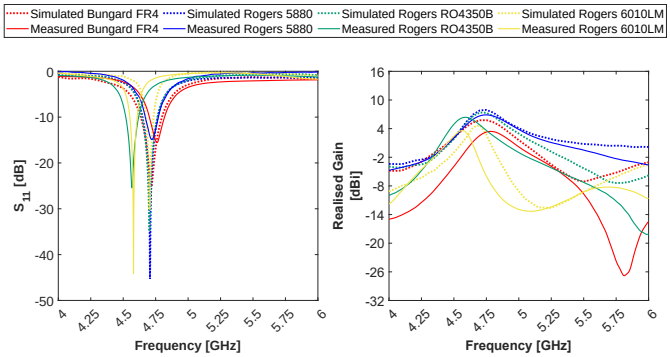

Figure 9: Simulated and measured S_{11} and realised gain for the laminate patch antennas.

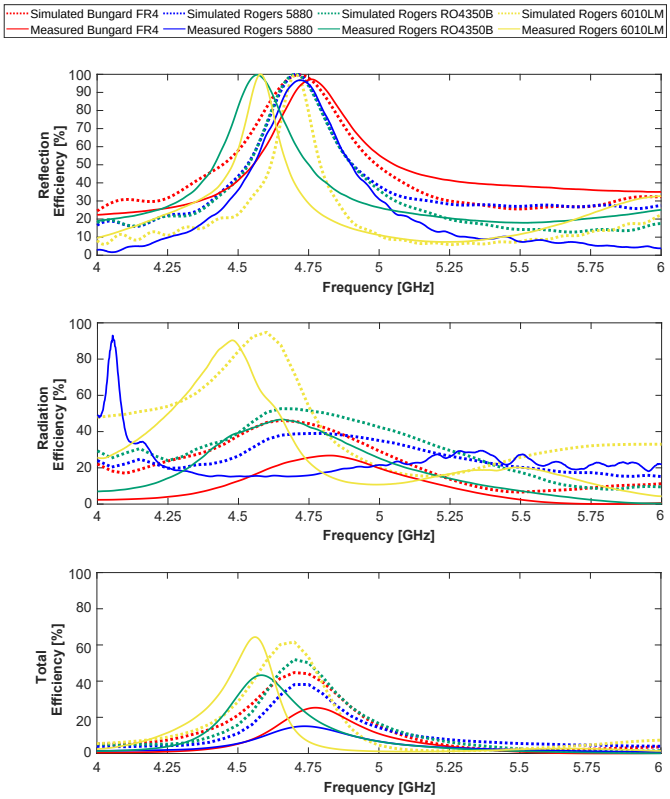

Figure 10: Simulated and measured reflection, radiation and total efficiencies for the laminate patch antennas.

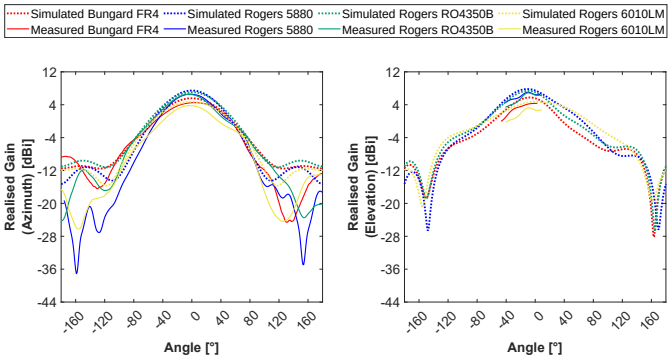

Figure 11: Simulated and measured azimuth (left) and elevation (right) cross-sections of the radiation pattern of the laminate patch antennas.

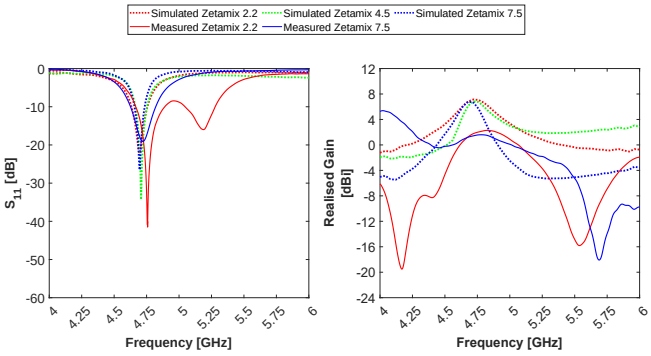

Figure 12: Simulated and measured S_{11} and realised gain for the 3D printed Zetamix patch antennas.

Table 4: Summary of the simulations and measurements results for the laminate patch antennas.

Antenna Reference	Frequency (GHz)	Bandwidth (GHz)	Peak Total Efficiency (%)	Peak Realised Gain (dBi)
Simulated A1	4.716	4.64 – 4.80	44.74	5.75
Measured A1	4.761	4.70 – 4.82	25.31	4.76
Simulated A2	4.706	4.65 – 4.77	38.09	7.82
Measured A2	4.719	4.67 – 4.77	15.07	6.80
Simulated A3	4.702	4.65 – 4.77	51.94	7.38
Measured A3	4.568	4.52 – 4.62	43.30	6.29
Simulated A4	4.704	4.66 – 4.74	61.64	4.71
Measured A4	4.580	4.55 – 4.61	64.35	3.46

measurements of the laminate patch antennas show close agreement with the simulations. The most notable discrepancies appear in the sidelobe regions of the Rogers RT/duroid 5880 and Rogers 6010LM patch antennas, where the measured sidelobe levels are lower than those predicted, as illustrated in Fig. 11. A summary of the simulation and measurement results for the laminate patch antennas is presented in Table 4.

4.2. 3D Printed Patch Antennas

Compared to the laminate-based antennas, the 3D printed patch antennas exhibit larger manufacturing variations. These arise primarily from the manual fabrication process of the patch and transmission line elements, which depends on both the precision of the mould and the accuracy of manual cutting. Additionally, the soldering of connectors introduces further inconsistencies, particularly affecting the 3D printed substrate around the SMA connector due to localised heating. The inherently rougher surface finish of 3D printed materials, relative to laminates, may also contribute to performance irregularities.

Unexpectedly, the patch antennas fabricated with Nanoe's Zetamix materials showed the weakest performance among all tested designs. Although their resonances occur near the intended frequency of 4.7 GHz with acceptable matching, the realised gain in this region is extremely low, indicating poor radiation efficiency. Interestingly, the Zetamix $\varepsilon = 7.5$ patch antenna exhibited notable gain near 4 GHz; however, the antenna exhibits poor impedance matching in that region. The simulated and measured S_{11} and realised gain for the Zetamix patch antennas are shown in Fig. 12.

As a result of the factors discussed above, the radiation efficiency of the antennas is significantly degraded, despite the reflection efficiency showing reasonable agreement with simulations. This reduction in radiation efficiency leads to a corresponding drop in total efficiency (Fig.13), thereby impacting the overall antenna performance.

One contributing factor to the observed deviations is the material behaviour of the filaments used. At room temperature, the filaments, particularly the Zetamix $\varepsilon = 7.5$, are extremely brittle. Successful fabrication requires a high and stable enclosure temperature in addition to an elevated extrusion temperature. Even when printed at the recommended temperature, the surrounding enclosure air may not have maintained adequate thermal stability. Consequently, the substrates remained fragile after the 3D printing process.

The azimuth and elevation radiation pattern cross-sections, shown in Fig. 14, reveal a highly erratic and flat-like response, indicating dispersed radiation and reduced directivity. This suggests that the Zetamix antennas operate with low efficiency as radiators, and may instead dissipate more power as heat than as directed electromagnetic energy.

The remaining manually fabricated antennas, A5 to A8, using PETG and PLA substrates, demonstrate acceptable performance, generally aligning well with simulation results. Deviations may stem from several factors, including limited resolution in cutting the radiating elements (copper foil and silver tape), imprecise soldering of SMA connectors to the feed lines, imperfect attachment of elements to the 3D printed substrates, and variations in the dielectric properties of the materials.

The S_{11} response, which shows multiple resonances, corresponds to the silver-coated patch with added silver tape on the ground plane. This is likely due to air gaps and leakage between the coated and taped ground planes, causing some radiation leakage. Despite the lack of deep resonances, all measured peaks are below -10 dB, indicating good matching. The realised gain is relatively high across the antennas, considering the fabrication process, with the silver-coated patch performing the worst. The simulated and measured S_{11} and realised gain of the PETG and PLA patch antennas are presented in Fig. 15.

The simulations and measurements of reflection and radiation efficiencies (Fig.16) show good agreement. The total efficiency for the PETG and PLA patch antennas is diminished

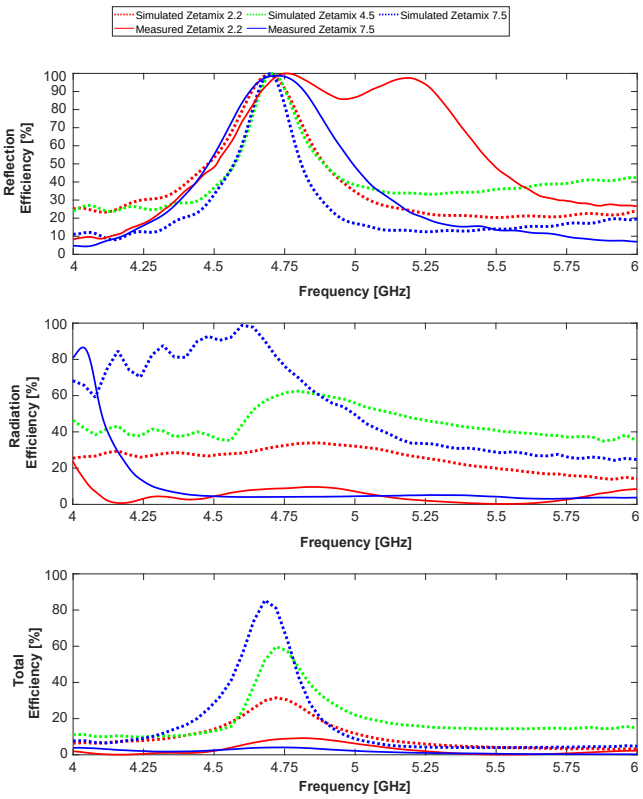

Figure 13: Simulated and measured reflection, radiation and total efficiencies for the 3D printed Zetamix patch antennas.

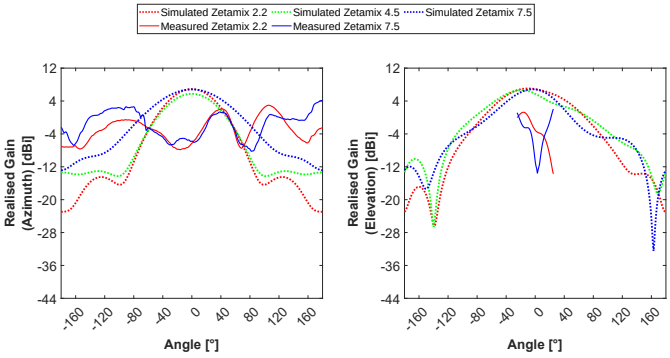

Figure 14: Simulated and measured azimuth (left) and elevation (right) cross-sections of the radiation pattern of the Zetamix patch antennas.

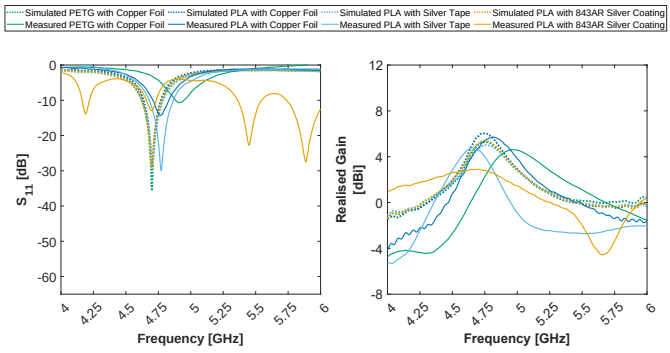

Figure 15: Simulated and measured S_{11} and realised gain for the 3D printed PETG and PLA patch antennas.

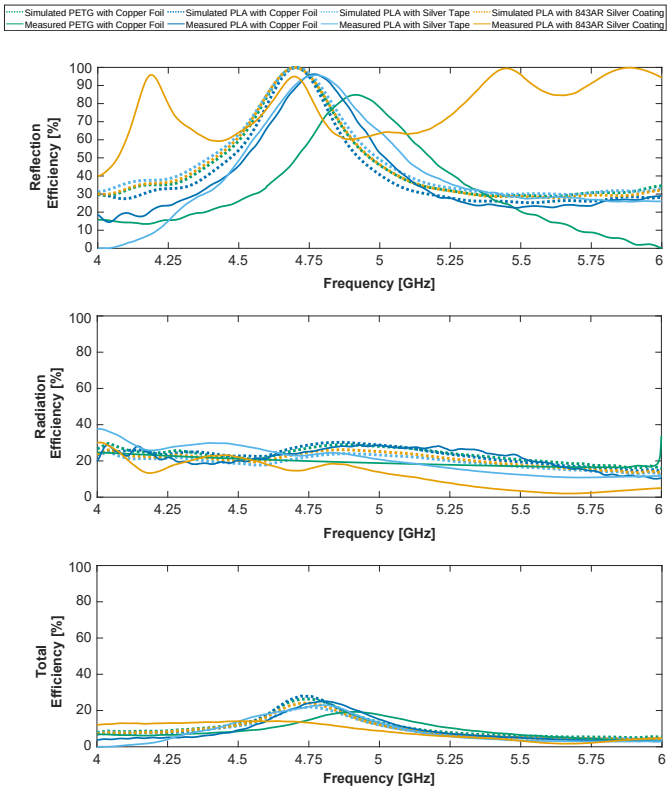

Figure 16: Simulated and measured reflection and radiation efficiencies for the 3D printed PETG and PLA patch antennas.

as a result of the decreased radiation efficiency. As expected, the silver-coated patch antenna shows the lowest efficiency, in line with the previously mentioned factors.

The azimuth and elevation cross-section radiation pattern measurements for the PETG and PLA patch antennas show good agreement with simulations. The most notable deviations from the expected patterns are one again observed in the silver-coated patch antenna, followed by the silver tape patch antenna, as illustrated in Fig. 17. A summary of the simulation and measurement results for the FDM 3D printed patch antennas is provided in Table 5.

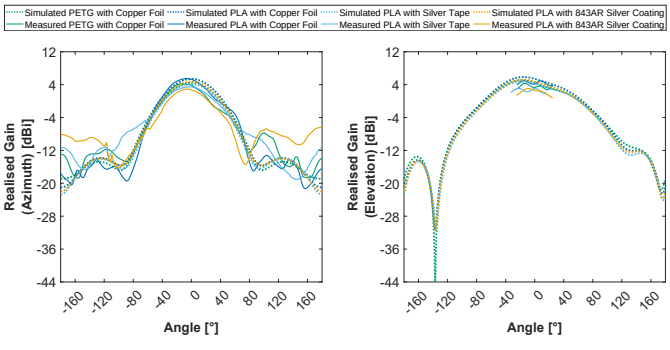

Figure 17: Simulated and measured azimuth (left) and elevation (right) cross-sections of the radiation pattern of the PETG and PLA patch antennas.

Table 5: Summary of the simulation and measurement results for the FDM 3D printed patch antennas.

Antenna Reference	Frequency (GHz)	Bandwidth (GHz)	Peak Total Efficiency(%)	Peak Realised Gain (dBi)
Simulated A5 †	4.700	4.63 – 4.78	26.30	5.04
Measured A5 †	4.914	4.88 – 4.95	19.26	4.46
Simulated A6 †	4.702	4.64 – 4.77	27.94	5.82
Measured A6 †	4.768	4.71 – 4.83	24.45	5.51
Simulated A7 ‡	4.706	4.62 – 4.79	21.56	4.74
Measured A7 ‡	4.772	4.68 – 4.87	22.64	3.64
Simulated A8 §	4.700	4.62 – 4.78	24.06	5.15
Measured A8 §	4.698	4.66 – 4.73	13.90	2.91
Simulated A9 †	4.696	4.63 – 4.76	31.40	6.96
Measured A9 †	4.758	4.67 – 4.89	9.54	2.02
Simulated A10 †	4.696	4.66 – 4.74	81.03	6.75
Measured A10 †	4.722	4.63 – 4.82	4.06	1.44
Simulated A11 †	4.708	4.66 – 4.75	59.77	6.64

† - metallisation with copper foil tape;
‡ - metallisation with silver conductive fabric cloth tape;
§ - metallisation with 843AR silver coating (simulation) and correction of the silver-coated ground plane with silver conductive fabric cloth tape (measurement).

5. Fabrication and Cost Analysis

To assess the feasibility of additive manufacturing (AM) as an alternative to conventional PCB-based fabrication, a cost comparison was conducted between the 3D printed patch antennas and their laminate-based counterparts. Table 6 summarises the estimated material costs, required equipment, and fabrication complexity for each antenna prototype discussed in this study.

While laminate-based antennas, particularly those fabricated on high-performance substrates such as Rogers RT/duroid 5880 or RO4350B, exhibit superior RF characteristics (as observed in last section), they also require specialised processes (e.g., UV exposure and chemical etching) and are significantly more expensive. In contrast, 3D printed antennas, especially those produced using widely available materials like PLA or PETG and metallised with copper foil, can be fabricated at a fraction of the cost using basic desktop equipment.

This cost-effectiveness also makes AM a valuable approach for developing low-budget antennas, ideal for hands-on teaching applications and for deployment in resource-limited regions or developing countries. Moreover, the flexibility and speed of 3D printing support rapid prototyping and geometrical customization, positioning it as a promising alternative for future antenna development in scenarios where affordability and accessibility are key drivers.

6. Conclusions

This study successfully fabricated and evaluated a range of patch antennas suitable for 5G applications using both laminate and 3D printing techniques. Two types of patch antennas were created: laminate-based patch antennas and 3D printed patch antennas. The laminate-based antennas used Bungard FR4 and three different Rogers laminates, while the 3D printed antennas were made with various materials, including Nanoe's Zetamix ε, Fiberlogy Easy PETG Black, and PLA Graphite. Different metallisation methods were tested for the 3D printed antennas, including copper foil tape, silver conductive fabric cloth tape, and silver coating for the conductive and radiative parts (e.g., patch, feed line, and ground plane).

The laminate-based antennas used the inset feed matching technique, while the 3D printed antennas employed the $\lambda/4$ transformer due to the complexity of manually implementing the inset feed.

Antenna parameters were evaluated with a focus on S_{11}, impedance bandwidth, peak total efficiency, and peak realised gain. While laminate-based antennas exhibited the best performance overall, the 3D printed antennas faced some challenges. Discrepancies between simulated and measured results were observed, mainly due to manufacturing errors and the precision of manual fabrication. The rougher surface of 3D printed parts compared to laminates introduced additional irregularities, which affected measurement reliability. In particular, the Nanoe Zetamix ε antennas performed the worst, showing significant deviations from designed resonances and lower efficiency. This likely stems from the intrinsic properties of the filament and the need for higher extrusion and enclosure temperatures than usual. Despite this, the remaining 3D printed antennas, particularly those using the PLA substrate with a copper foil patch, showed acceptable results.

The precision of fabrication through etching and the smoothness of dielectric substrates with copper cladding contributed to the superior performance of the laminate-based antennas. As anticipated, the 3D printed antennas had some limitations in terms of resonance accuracy and realised gain, but the PETG and PLA antennas still showed promising results. To improve the performance of 3D printed antennas, additional processing steps, such as smoothing before metallisation with coatings or foils (e.g., sanding or vapour smoothing), are necessary.

While laminate-based antennas proved to be more effective for high-frequency applications, 3D printing offers significant advantages in rapid prototyping and customisation. The ability to quickly fabricate complex antenna structures, tailored to specific performance requirements, is one of the key benefits of 3D printing. For more complex designs with intricate features, 3D printing provides flexibility in material selection and design modifications, making it a promising alternative for advanced antenna applications, particularly where prototyping speed and geometric complexity are critical.

Future work should focus on optimising 3D printing parameters and exploring new materials to enhance both the mechanical and dielectric properties (as e.g. ABS or other filaments with dielectric properties closer to Rogers substrates) of 3D printed antennas. Moreover, the potential integration of conductive filaments will be explored, as this could simplify or even eliminate post-metallisation steps, enhancing fabrication efficiency. However, the key to bridging the performance gap between traditional laminate-based techniques and 3D printed substrates will likely lie in the development of more precise metallisation techniques."

Acknowledgments

This work was supported in part by Portugal PRR – Plano de Recuperação e Resiliência (The Recovery and Resilience Plan), under Project INOV.AM - Innovation in Additive Manufacturing; in part by FCT - Fundação para a Ciência e Tecnologia,

Table 6: Estimated cost comparison between 3D Printed and Laminate-based patch antennas (per unit)

Antenna	Substrate	Metallisation Method	Cost (€)	Equipment Required	Complexity	Remarks
A1	FR4	Copper cladding	1.50–3.00	UV exposure, etching setup	Moderate	Low-cost. Low RF performance at high frequencies
A2	Rogers 5880	Copper cladding	20–40	Same as above	Moderate	Excellent RF performance
A3	Rogers RO4350B	Copper cladding	15–30	Same as above	Moderate	Balanced cost/performance
A4	Rogers 6010LM	Copper cladding	30–60	Same as above	Moderate	High permittivity, costly
A5	PETG	Copper foil tape	∼2.50	FDM printer, cutter	Low	Very affordable
A6	PLA	Copper foil tape	∼2.00	Same as above	Low	Cheapest combination
A7	PLA	Silver fabric tape	∼4.00	Same as above	Low	Flexible metallisation
A8	PLA	Silver spray (843AR)	∼8.00	Same as above	Low–Mod.	Uneven coating risk
A9	Zetamix $\varepsilon_r = 2.2$	Copper foil tape	16–21	High-temp 3D printer	Mod.–High	Brittle material
A10	Zetamix $\varepsilon_r = 7.5$	Copper foil tape	21–26	Same as above	High	Weakest performance/cost

I.P. by project reference 10.54499/UIDB/50008/2020 and DOI identifier https://doi.org/10.54499/UIDB/50008/2020; and in part by FCT under Project LA/P/0109/2020.

References

[1] F. Pizarro, R. Salazar, E. Rajo-Iglesias, M. Rodríguez, S. Fingerhuth, and G. Hermosilla, "Parametric Study of 3D Additive Printing Parameters Using Conductive Filaments on Microwave Topologies," *IEEE Access*, vol. 7, pp. 106 814–106 823, 2019.

[2] S. Zhang, R. K. Arya, W. G. Whittow, D. Cadman, R. Mittra, and J. C. Vardaxoglou, "Ultra-Wideband Flat Metamaterial GRIN Lenses Assisted With Additive Manufacturing Technique," *IEEE Transactions on Antennas and Propagation*, vol. 69, no. 7, pp. 3788–3799, 2021.

[3] Q. Wang, X. Han, P. Yu, J.-Q. Hou, and Z.-Y. Lei, "A 3d-printed spherical dual-circular polarized luneburg lens antenna for ku-band," *IEEE Access*, vol. 13, pp. 19 110–19 117, 2025.

[4] J. R. Reis, C. Ribeiro, and R. F. S. Caldeirinha, "Compact 3D-printed reflector antenna for radar applications at K-band," *IET Microwaves, Antennas & Propagation*, vol. 15, no. 8, pp. 843–854, 2021.

[5] B. Nie, H. Lu, T. Skaik, Y. Liu, and Y. Wang, "A 3D-Printed Subterahertz Metallic Surface-Wave Luneburg Lens Multibeam Antenna," *IEEE Transactions on Terahertz Science and Technology*, vol. 13, no. 3, pp. 297–301, 2023.

[6] C. Stoumpos, T. L. Gouguec, R. Allanic, M. García-Vigueras, and A.-C. Amiaud, "Compact Additively Manufactured Conformal Slotted Waveguide Antenna Array," *IEEE Antennas and Wireless Propagation Letters*, vol. 22, no. 8, pp. 1843–1847, 2023.

[7] D. Mair, M. Renzler, S. Kovar, T. Martinek, T. Kadavy, S. Bergmueller, A. Horn, J. Braun, and L. Kaserer, "Evolutionary Optimized 3D WiFi Antennas Manufactured via Laser Powder Bed Fusion," *IEEE Access*, vol. 11, pp. 121 914–121 923, 2023.

[8] Y. Bi, Y. Li, and J. Wang, "3-D Printed Wideband Cassegrain Antenna With a Concave Subreflector for 5G Millimeter-Wave 2-D Multibeam Applications," *IEEE Transactions on Antennas and Propagation*, vol. 68, no. 6, pp. 4362–4371, 2020.

[9] X. Guo, Q. Chen, X. Zhou, M. Chai, Z. Huang, L. Yang, and Y. Li, "A miniaturized low-weight 2.4 ghz circularly polarized antenna using 3d printing technology," *IEEE Access*, vol. 12, pp. 195 464–195 471, 2024.

[10] R. Shamsaee Malfajani, R. Damansabz, S. Bodkhe, D. Therriault, J.-J. Laurin, and M. S. Sharawi, "3-d-printed encapsulated dielectric resonator antennas with large operation frequency ratio for future wireless communications," *IEEE Open Journal of Antennas and Propagation*, vol. 5, no. 5, pp. 1351–1364, 2024.

[11] B. Kattel, W. E. Hutchcraft, and R. K. Gordon, "Evaluating the relationship between relative permittivity and infill density in 3d printed dielectric slabs," *IEEE Access*, vol. 13, pp. 16 171–16 181, 2025.

[12] S. S. Carvalho, J. R. V. Reis, A. Mateus, and R. F. S. Caldeirinha, "Exploring Design Approaches for 3D Printed Antennas," *IEEE Access*, vol. 12, pp. 10 718–10 735, 2024.

[13] S. S. Carvalho, J. R. V. Reis, and R. F. S. Caldeirinha, "A State-of-the-Art Review on 4D Printed Antennas and Other Adaptable Designs," *IEEE Access*, vol. 12, pp. 62 861–62 881, 2024.

[14] C. A. Balanis, *Antenna Theory: Analysis and Design*, 4th ed. John Wiley & Sons, Feb. 2016.

[15] Rohde & Schwarz, "Measurement of Dielectric Material Properties - Application Note," Apr 2012.

[16] K. Y. You, "Materials Characterization Using Microwave Waveguide System," in *Microwave Systems and Applications*, S. K. Goudos, Ed. Rijeka: IntechOpen, 2017, ch. 14.

[17] A. Gilmour, *Microwave Tubes*, ser. Artech House microwave library. Artech House, 1986.

[18] MG Chemicals, "843AR Aerosol Super Shield Silver Coated Copper Conductive Spray Paint," Tech. Rep.

[19] 3M, "3M Fabric Tape AG-2300 Conductive Silver Fabric."

[20] EMI Thermal, "Conductive Cloth Tape Datasheet."